Real-Time Morphological Observation of Isotactic Polypropylene and Poly(ethylene-*co*-octene) Rubber Blend during Temperature Change

Michio Ono,[1,2]* Ken Nakajima,[2] Mayumi Misawa,[3] Toshio Nishi[2]

[1]*SunAllomer Ltd., Kawasaki Development Center, Kawasaki-Ku, Kawasaki, Kanagawa 210-0863, Japan*
[2]*Department of Organic and Polymeric Materials, Faculty of Engineering, Tokyo Institute of Technology, Meguro-Ku, Tokyo 152-8552, Japan*
[3]*Nihon Veeco K. K., Application Group Metrology, Chuou-Ku, Tokyo104-0045 Japan*

Received 23 August 2007; accepted 20 November 2007
DOI 10.1002/app.27803
Published online 29 January 2008 in Wiley InterScience (www.interscience.wiley.com).

ABSTRACT: In the injection- and compression-molded specimens composed of isotactic polypropylene (iPP) and poly(ethylene-*co*-octene) rubber (EOR) blend, its morphological changes with temperature variation were investigated using an atomic force microscopy equipped with a heater accessory. Phase-separated sea-island structures comprising the iPP matrix (sea) and the EOR domains (island) were clearly observed in both specimens. In the injection-molded specimen, the morphology of the EOR domains was fibrous along flow direction (FD). In the iPP matrix, a stripe-like structure consisting of alternating iPP crystalline lamellae and amorphous region was clearly observed at room temperature. As increasing temperatures, the iPP amorphous regions seemed to shrink gradually and could not be identified at 80°C. By contrast, in the compression-molded specimen, the EOR domains were circular in shape, and the alternate structure comprising the iPP crystal lamellae and amorphous regions was also found. At elevated temperatures, the iPP amorphous regions gradually enlarged. The analysis of the apparent activation energy obtained by a dynamic mechanical thermal analysis revealed that the differences in the morphological behavior in the iPP matrix region between the both specimens were attributed to the differences in the mobility in the iPP crystal regions. © 2008 Wiley Periodicals, Inc. J Appl Polym Sci 108: 1857–1864, 2008

Key words: polypropylene (PP); atomic force microscopy (AFM); injection molding

INTRODUCTION

Isotactic polypropylene (iPP) is outstanding among other polymers because of its price/mechanical properties balance, easy processability, and good wetherability.[1] Hence, it has been in wide use of many fields such as automobile, consumer products, sheets and textile processed by injection, blow, extrusion, and spinning. The iPP has been usually used in the form of polymer alloy by being melt-blended with various thermoplastic elastomers (TPEs) to improve brittle impact properties.[2–6]

In particular, the iPP/TPE alloys have been widely applied to injection-molded parts in automobile industry. These parts are usually subjected to be quite severe thermal conditions ranging from less than −30°C for the exterior parts to more than ~ 80°C for the interior ones. It is known that such a temperature change has a great influence on some properties, impact strength,[2,4,6] Young's modulus,[7] and linear thermal expansion coefficient.[8–11] The mechanism of the change in the physical properties toward temperature change has not been fully understood. This is mainly because of lack of the information about the real-time morphological change toward temperature variation.

In this study, using an atomic force microscopy (AFM), we investigated the morphological changes with temperature variation for the specimens composed of iPP and poly(ethylene-*co*-octene) rubber (EOR) blend fabricated by two different molding methods, injection- and compression molding. It was found that the interlamella morphologies in the iPP matrix changed quite differently between the injection and the compression specimen at elevated temperatures.

**Present address:* Dow Japan Development Center, Dow Chemical Japan Ltd., 8-1, Ukishima-Cho, Kawasaki-Ku, Kawasaki-Shi, Kanagawa-Ken, 210-0862, Japan.
Correspondence to: M. Ono (mono@dow.com)

Journal of Applied Polymer Science, Vol. 108, 1857–1864 (2008)

EXPERIMENTAL

Raw material and specimen preparation

Isotactic polypropylene (iPP) used in this study, which was kindly supplied by SunAllomer, had 5600 Pa s of a zero shear viscosity (η^*_m) at 210°C,

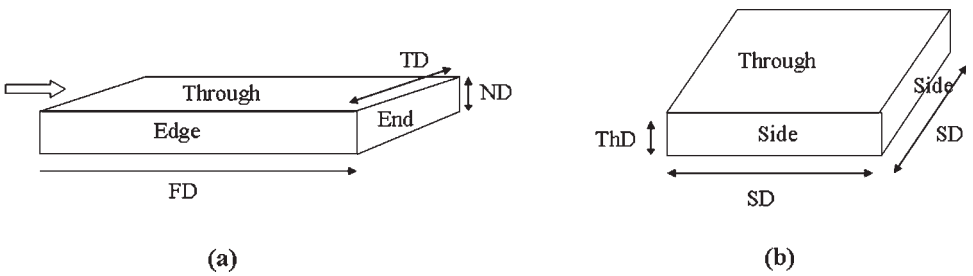

Figure 1 Definition of the directions and cross-sections. (a) Injection-molded specimen designated as Blend-I. For directions, FD, TD, and ND are parallel to flow, transverse-to-flow, and normal direction, respectively. For cross-sections, edge-, end-, and through-view are the cross-section parallel to FD, TD, and ND, respectively, and (b) compression-molded specimen designated as Blend-P. For direction, SD and ThD are parallel to length (width) direction and thickness direction, respectively. For cross-sections, side- and through-view are the cross-section parallel to SD and ThD, respectively.

98.5% of isotactic index on the basis of pentad sequences [mmmm] determined by ^{13}C NMR and 165°C of melting temperature with differential scanning calorimeter (DSC) at a scanning rate of 10°C/min. Poly(ethylene-*co*-octene) rubber (EOR), which was purchased from Dow Chemical, had 24 wt % of octene contents, 455 Pa s of zero shear viscosity (η_i^*) at 210°C, 55°C of melting temperature by DSC.

The blend sample with a composition of 70/30 (v/v) of iPP/EOR having 0.085 of a viscosity ratio η_i^*/η_m^* was prepared by melt blending with a corotating twin-screw extruder (TEX30α; Japan Steel Works, Tokyo, Japan) at 180°C in barrel temperatures. The resulting blend was fabricated to obtain two types of slab-shaped specimens by different two molding methods: injection- and compression molding. The injection-molded specimen was obtained with an injection machine (Fanuc α100C; Funac, Toyama, Japan) under the following conditions: 200°C of cylinder setting temperatures, 40°C of cooling temperature, and 2.8 s of injection time to full package. The compression-molded one was prepared by plasticizing at 230°C for 5 min followed by hot-pressing under 10 MPa and then by cooled at 30°C under 5 MPa. Each specimen was designated as Blend-I for the injection-molded specimen and Blend-P for the compression-molded one. The directions and the cross-sections of both specimens were designated in Figure 1. The each slab was annealed at 100°C for more than 24 h to remove a residual stress. Thus, the influences of excess expansion due to relieving stress at elevated temperatures will be neglected.

Morphological observation during temperature change

Morphological changes at various temperatures of room temperature (~ 23°C), 40, 60, 80, 100 and the room temperature rapidly cooled from 100°C, were observed using an atomic force microscope (AFM) (Nanoscope IV MultiMode AFM; Veeco, New York) equipped with a high-temperature heater accessory. The measurement was started after keeping each test temperature for 20 min which would be long enough to make the sample and the cantilever reach to the test temperature.[12] The AFM images were taken in tapping mode using a silicone cantilever with a spring constant of 2.8 N/m and resonance frequency of 75 kHz. Both height and phase images were taken simultaneously. All data were collected with 512 × 512 pixels per image. Typical scan rates, set point amplitude ratio and scan size during recording were 1.0 Hz, 0.7–0.8, and 500 × 500 nm^2, respectively. The flat surfaces for the AFM measurements, which were taken from a core layer, were obtained by cryomicrotomed at −100°C with a diamond knife. Note that the observation by AFM was carried out in a core layer not a skin layer. The AFM observation was carried out in the edge view of Blend-I and the side view of Blend-P.

Evaluation of molecular mobility by apparent activation energy

The molecular mobility of the amorphous or the crystalline region of the iPP in the blend was evaluated on the basis of the apparent activation energy of each region. It was obtained by the linear dynamic mechanical analysis using a dynamic mechanical thermoanalyzer (DMTA) (RSAIII; TA Instruments) on a tensile mode. The rectangular specimen with 30 (length) by 3.0 (width) by 0.4 (thickness) mm^3 was cut out from the slab and mounted in a sample holder in such a way that the ''length'' direction, thus the oscillatory strain direction, coincided with the FD or the SD. The loss moduli, E'', were monitored ranging from −80 to 140°C at various frequencies, f, of 0.5, 1.0, 2.0, 5.0, 10, and 50 Hz, and at a heating rate of 4.0°C/min. The dispersion peaks associated with the iPP molecular motion were observed at around 0 and 80°C. The peak at around 0°C was the primary dispersion, α_a, ascribed to the micro-Brownian motion of amorphous chains and the higher peak (80°C) belonged to the crystalline

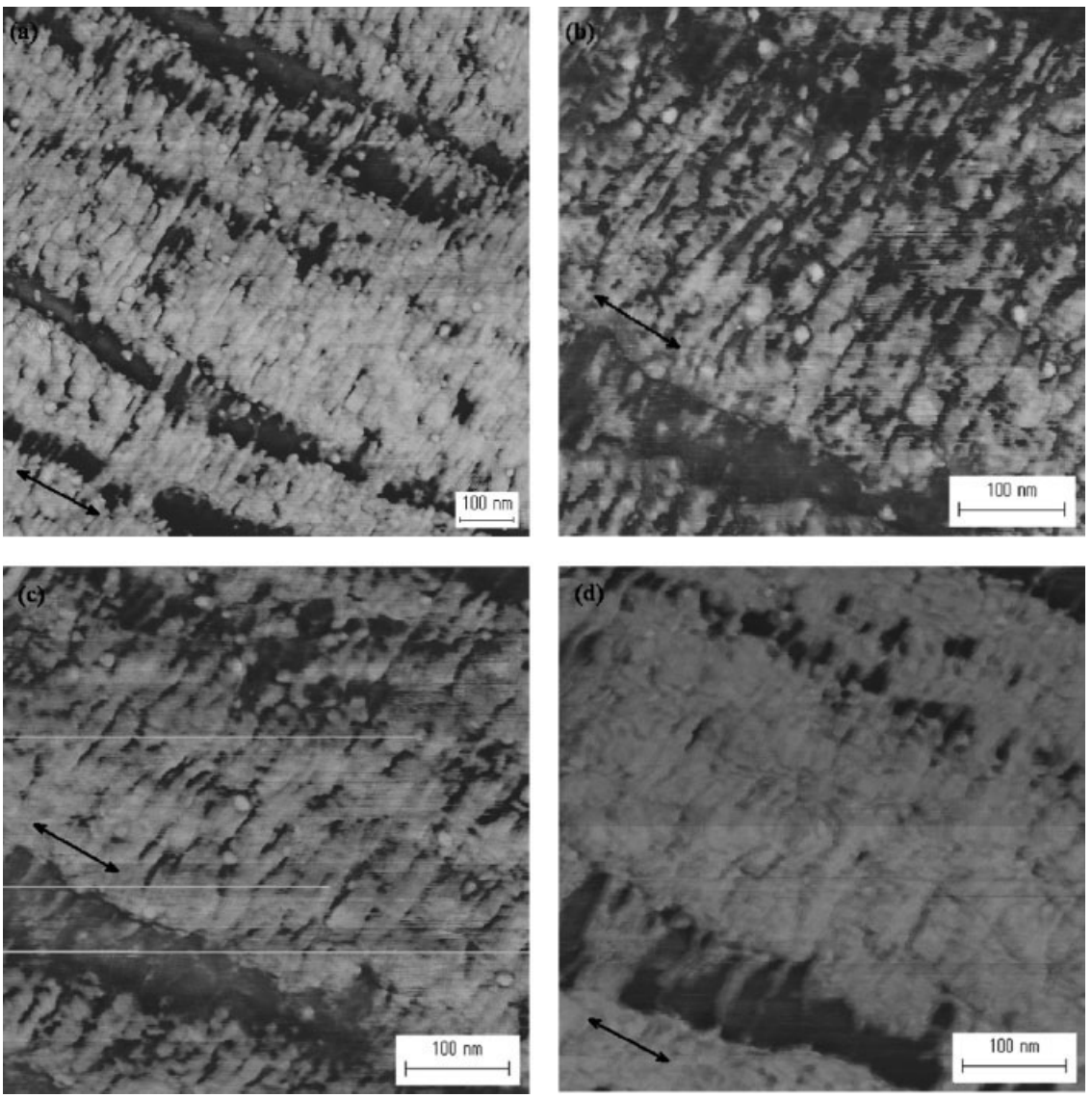

Figure 2 AFM phase images for Blend-I at room temperature at low magnification (a), at higher magnification (b), at 40°C (c), at 60°C (d), at 80°C (e), at 100°C (f), and at the room temperature cooled rapidly from 100°C (g), respectively. The arrows indicate the FD.

dispersion, α_c, caused by internal friction within the crystalline region.[13,14] The apparent activation energy, ΔH^*, of the iPP amorphous or crystalline region was given by inserting a gradient from the plot of log f as a function of reciprocal temperature, $1/T$, of the corresponding E'' peak to the α_a or the α_c at a given frequency, f, into eq. (1).[15]

$$\Delta H^* = -2.303R \frac{d \log f}{d(\frac{1}{T})} \quad (1)$$

Here, R denotes gas constant, 8.31 J/(K mol).

Thermal properties

The thermal properties of the samples were evaluated differential scanning calorimeter (DSC) (DSC7; Perkin-Elmer, Waltham, MA). The specimen used (5–7 mg) was cut out from each Belnd-I or -P and sealed in an aluminum pan. The first scan heating was carried out from −30 to 230°C at a rate of 10°C/min. After the first scan, the sample was held at 230°C for 5 min, cooled down to −30°C at a rate of 10°C/min, and then reheated until 230°C at a rate of 10°C/min (the second heating scan). Both the heating profiles by the first and second scan were recorded.

RESULTS AND DISCUSSION

Differences in the morphological behaviors between the injection and compression-molded specimens at higher temperatures by AFM

Figure 2 shows AFM phase images of Blend-I at various temperatures. In general, the phase contrast is

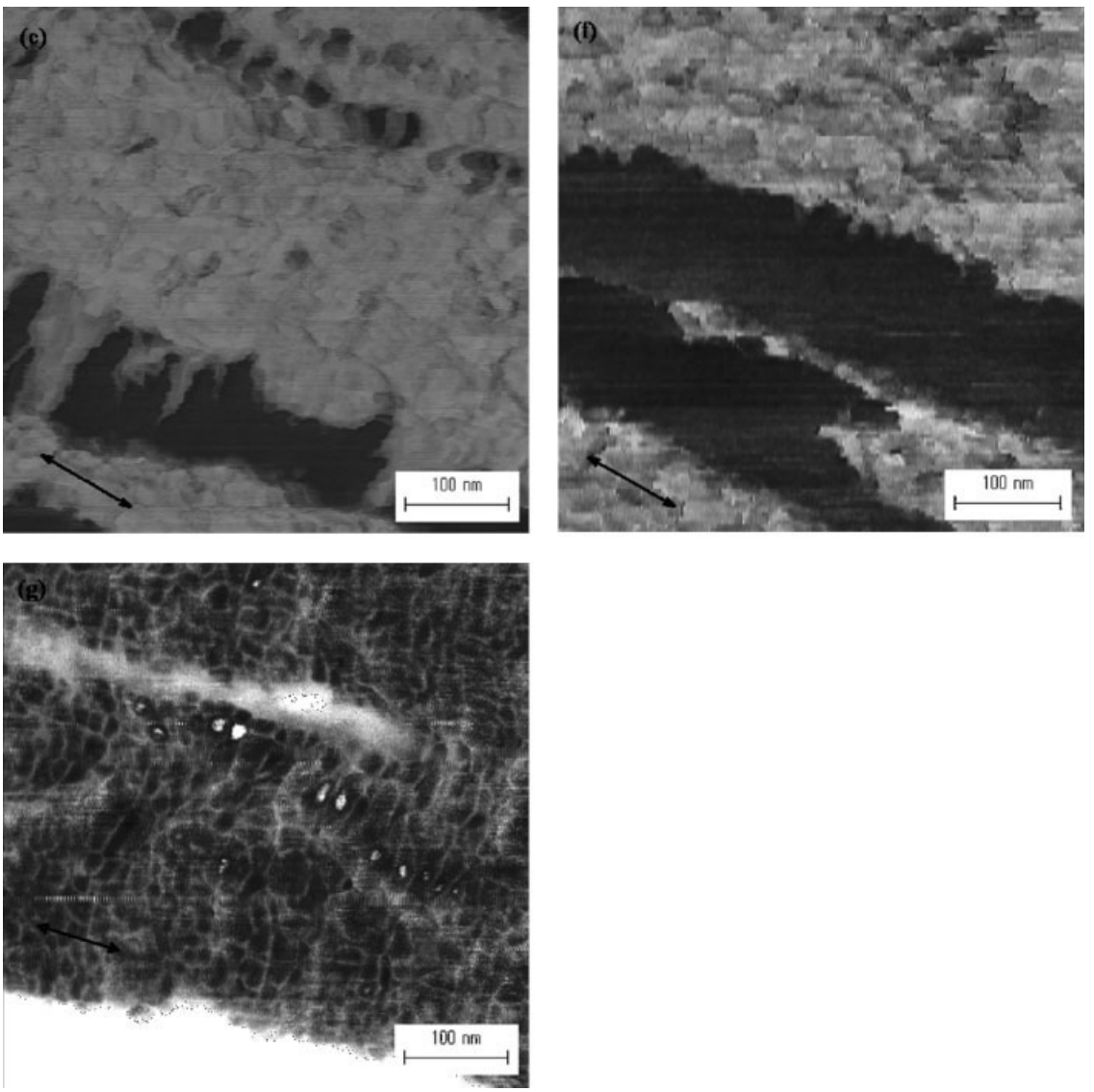

Figure 2 (*Continued from the previous page*)

obtained because of the phase lag and frequency shift of the cantilever oscillation relative to drive signal of the cantilever. In these figures, except for Figure 2(g), where inverse trend of the phase contrast is found, dark regions represent soft or adhesive regions as a result of the phase lag and thus bright regions indicate hard or low adhesive regions.

At low magnification [Fig. 2(a)] at room temperature, a sea-island structure comprising fibrous dark regions (island) and bright regions (sea) is clearly observed in which the dark regions are highly deformed along the FD and they formed cocontinuous structures with the iPP matrix. The dark regions with more adhesive will correspond to EOR-rich phases resulting from phase-separation. In immiscible or partially miscible binary blends with less than 1.0 of a viscosity ratio, minor component having lower viscosity are highly deformed along FD and formed cocontinuous structures due to a given shear followed by an elongational force upon injection-molding process.[16–18] Our system is typical case in this pattern.

In bright regions, that is, iPP-rich phases, stripe patterns originating from iPP lamellae are clearly observed. These lamellae are aligned perpendicular to the deformed EOR-rich phases. This is in good agreement with the TEM picture in our previous report.[8]

At higher magnification [Fig. 2(b)], dark regions corresponding to the iPP amorphous regions in the iPP matrix can be clearly observed between the iPP lamellae. The interlamella distance (long period) is widely distributed from 15–17 to 25–40 nm.

When increasing temperature up to 40°C [Fig. 2(c)], there has little or no change in the EOR rich regions. However, the PP amorphous regions seem to shrink

to being narrower in their thickness. As successively increasing temperature up to 100°C [Fig. 2(d–f)], the shrinkage of the PP amorphous regions further accelerates and finally it cannot be confirmed at 100°C [Fig. 2(f)].

When cooling down to room temperature from 100°C [Fig. 2(g)], the phase contrast is inverted, that is, the EO- and the iPP-rich phase appear as the bright and the dark region, respectively. In addition, a mesh-like structure consisting of streaks parallel both to FD and TD is formed. Such phase inversion might be interpreted as the ''edge effect'' caused by a phase inversion as a result of a fact that a tip contacts with large bumps (the EOR phases subjected to successive melt and solidification) or as the change in a tip-sample interaction because of a molten EOR deposition on the tip.

On the other hand, the morphological behaviors in the Blend-P [Fig. 3(a–f)] are quite different from those in the Blend-I. At room temperature [Fig. 3(a)], the EOR phases (dark regions) are spherical in shape and the iPP lamellae are randomly oriented.

On gradually increasing temperatures up to 60°C [Fig. 3(b,c)], little or no changes in the iPP-rich region are found. On further increase in temperature at 80 and 100°C [Fig. 3(d,e)], we can observe the increase in the dark regions in the iPP phase, that is, the iPP amorphous regions. This is reasonable result, considering that the thermal expansion in the iPP amorphous region is much higher than that in the PP crystalline regions,[19] thus resulting in enlargement of the iPP amorphous regions as increasing temperatures.

Interpretation of AFM image differences between Blend-I and -P at higher temperatures

In this section, we will try to elucidate decrease in the amorphous regions in the interlamellae in the iPP matrix in the Blend-I at elevated temperatures. The following hypotheses are considered: (1) shrinkage of the iPP amorphous region by the retraction form taut tie molecules at higher temperatures,[20,21] resulting in the decrease in the iPP amorphous region, (2) increase in the crystallinity by secondary crystallization to expand the iPP crystal region (to render the iPP amorphous region shrink), and (3) the iPP crystal chains to be softening (or melt) below the T_m of the iPP caused by easier molecular mobility of the iPP crystal chains, which will make the crystal region as adhesive as the amorphous region and thus will lead to making the interface between the crystal and amorphous regions in the lamellae of the iPP matrix unclear.

The first factor can be confirmed by the change in the long periods in the iPP interlamellae using a small angled X-ray analysis (SAXS) with variable temperatures. In the present case, the decrease in the long period in the interlamellae, thus shift in the scattering vector toward higher angles by temperature rise would be expected. However, little or no shift in it toward higher angles according as temperature rise was found in the SAXS experiment. Hence, this hypothesis was denied.

The second factor can be clarified by the change in the crystallinity in the iPP of the specimen annealed at different temperatures with no anneal, 40, 60, 80, and 100°C. The crystallinity change of the specimens at each annealing stage was obtained by the DSC analysis as follows: the specimen taken from the Blend-I or -P was heated to desired annealing temperature, then held at this temperature for 30 min and after that, reheated to 230°C at 10°C/min. Dividing the heat of fusion around the T_m ($\sim$ 165°C) by the one corresponding to the perfect crystalline iPP (209 J/g)[22] gave the crystallinity corresponding to the each annealing stage. In the present case, the increase in the crystallinity would be expected according as the increase in the annealing temperature (initial holding temperature). However, no major change in the crystallinity was found. Thus, the second factor was denied.

As for the molecular chain mobility as the third possibility, we compared the apparent activation energies, ΔH^*, of both the crystal (α_c) and the amorphous (α_a) chains in the iPP for the Blend-I with those for the Blend-P.

The relaxation peak of the α_a of the iPP in the blend was clearly observed at around 270–280 K. This peak was employed as it was for the determination of ΔH^* of the α_a. The relaxation peak of the α_c of the iPP was, however, observed as an inflection point around 350 K not a peak. Hence, we adopted the point of the intersection obtained by extrapolating the two tangent lines of the curve of DMTA as the relaxation peak of the α_c. An example is shown in Figure 4.

Arrhenius plots of log f and reciprocal T for the α_c and α_a are shown in Figure 5(a,b), respectively. Straight lines are obtained in both relaxations. Inserting the slope of these lines into eq. (1) yields the apparent activation energy (ΔH^*) of each blend. The value of the ΔH^* for the α_c is 95 kJ/mol for the Blend-I and 136 kJ/mol for the Blend-P, respectively, thus being indicative of higher mobility of the crystal regions for the injection-molded blend (Blend-I). On the other hand, the value of the ΔH^* for the α_a exhibits 396 kJ/mol for the Blend-I and 411 kJ/mol for the Blend-P, indicating no differences in the mobility in the iPP amorphous chains between the two blends.

Melting imperfect crystals even below the T_m of the iPP might be one of the responsible causes of such easier mobility of the crystal chains of the iPP

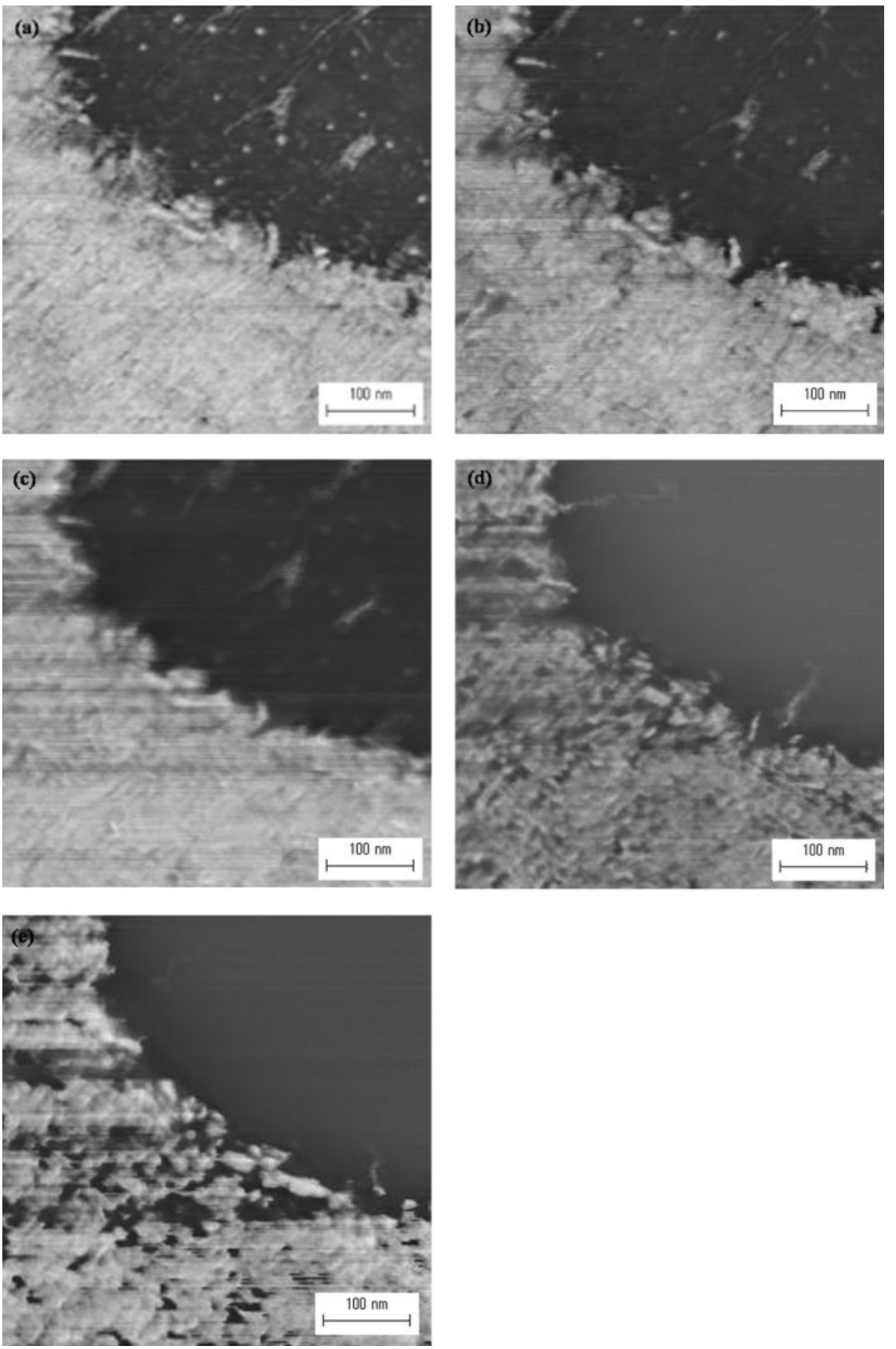

Figure 3 AFM phase images for Blend-P at room temperature (a), at 40°C (b), at 60°C (c), at 80°C (d), and at 100°C (e), respectively.

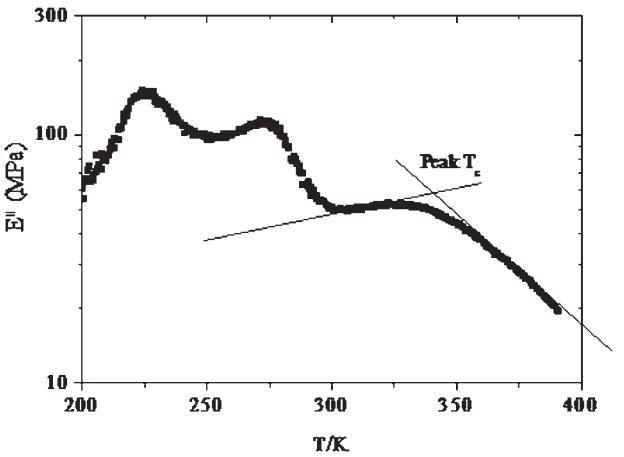

Figure 4 Determination of the crystal dispersion peak, α_c.

in the Blend-I. In fact, during an injection molding involving a process that melts inject into a cavity under a given shear and then rapidly solidify, a number of imperfect crystals of iPP might generate and such an imperfect crystal started to melt at around 40°C.[23]

Hence, we verify the presence of such imperfect crystals on the basis of the thermal analysis of the ''as-fabricated'' samples by DSC. The as-fabricated samples still involve its thermal histories and topological constraints which would be related with melting imperfect crystals. They would reflect on the first heating profile. In addition, the second heating profile exhibits the thermal information in the equilibrated state after eliminating the inherent thermal history. Thus, from the first scan profile and the second heating one, we can obtain the information on melting behavior of the imperfect crystals. The DSC profiles are shown in Figure 6(a: Blend-I) and (b: Blend-P), respectively.

In Figure 6(a), two peaks are clearly observed around 40°C (peak1) and 60°C (peak2). The peak around 60°C would correspond to the melting peak of crystal part of EOR because this is nearly consistent with the T_m of EOR and also remains as peak3 in the second heating scan. The peak1 around 40°C would then correspond to the T_m of the imperfect crystals of the iPP generating during injection-molding mentioned earlier.[23]

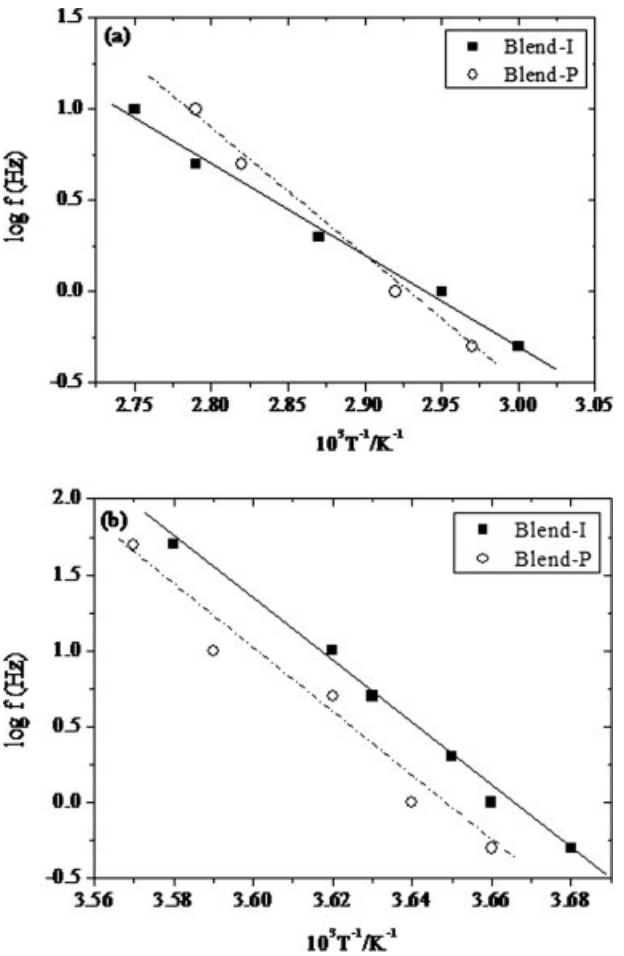

Figure 5 Log f as a function of reciprocal T for Blend-I and Blend-P; the crystal dispersion, α_c (a) and the primary dispersion, α_a (b), respectively.

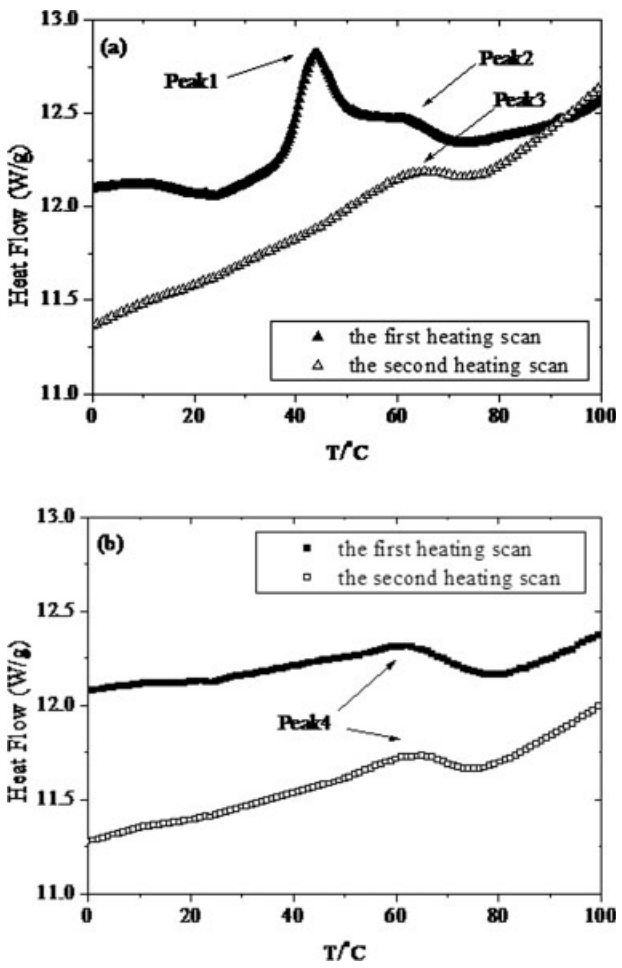

Figure 6 DSC heating profiles at around low temperature region for Blend-I (a) and Blend-P (b), respectively.

On the other hand, for the Blend-P as shown in Figure 6(b), no differences between the first and the second heating scan are found, where one peak (peak4) corresponding to the T_m of EOR crystal part is observed around 60°C. The cooling process in the compression-molding would proceed in a nearly equilibrated state because there would be less change in both shear rate and temperature compared with the injection-molding.

From the results obtained earlier, we will consider the AFM image difference between the two blends. In terms of the phase images on the tapping mode, the image contrast is discriminated as the difference in the adhesive force between tip and sample. In the case of the Blend-I, the melting in the imperfect crystals occurs more easily compared with the Blend-P, thus resulting in making the surface of crystal regions so adhesive as the amorphous regions and causing disappearance of the phase image contrast between the two regions at elevated temperatures. That would be one of the plausible reasons why the amorphous regions of the Blend-I seem to shrink and disappear at higher temperatures.

Furthermore, a temperature-variable AFM with thermal conductivity accessory, which would give more definitive information, is now under way and it will be reported as another article.

CONCLUSIONS

Using AFM, we carried out real-time morphological observations at elevated temperatures of two samples: injection-molded (Blend-I) and compression-molded (Blend-P) specimens with the same composition, iPP/EOR. When increasing in temperatures, the iPP amorphous regions between the interlamellae of the iPP matrix showed quite different behaviors between the Blend-I and -P. It seemed to get disappeared at 100°C for the Blend-I whereas to be expanded for the Blend-P. The expansion of the iPP amorphous regions in the Blend-P was interpreted as a result of higher thermal expansion of the iPP amorphous regions. On the other hand, the disappearance of them in the Blend-I was not due to real shrinkage of the amorphous regions but due to loss of the contrast between the amorphous and crystal regions caused by the melting of imperfect crystals of the iPP under the T_m. It made the crystal regions as adhesive as the amorphous ones, and thus made the interface between them unclear.

References

1. Moore, E. P., Jr. Polypropylene Handbook; Carl Hanser Verlag: Münich, Germany; 1996.
2. Van der Wal, A.; Nijhof, R.; Gaymans, R. J. Polymer 1999, 40, 6031.
3. Van der Wal, A.; Gaymans, R. J. Polymer 1999, 40, 6045.
4. Van der Wal, A.; Verheul, A. J. J.; Gaymans, R. J. Polymer 1999, 40, 6057.
5. Van der Wal, A.; Gaymans, R. J. Polymer 1999, 40, 6067.
6. Jang, B. Z.; Uhlmann, D. R.; Vander Sande, J. B. Polym Eng Sci 1985, 25, 643.
7. Copplola, F.; Greco, R.; Martuscelli, E.; Kammer, H. W.; Kummerlowe, C. Polymer 1987, 28, 47.
8. Ono, M.; Washiyama, J.; Nakajima, K.; Nishi, T. Polym J 2004, 36, 563.
9. Ono, M.; Washiyama, J.; Nakajima, K.; Nishi, T. Polymer 2005, 46, 4899.
10. Ono, M.; Nakajima, K.; Nishi, T. Kautschuk Gummi Kunstsoffe 2006, 11-06, 574.
11. Ono, M.; Nakajima, K.; Nishi, T. J Appl Polym Sci 2008, 107, 2930.
12. Ivanov, D. A.; Amalou, Z.; Magonov, S. N. Macromolecules 2001, 34, 8944.
13. Takayanagi, M.; Imada, K.; Kajiyama, T. J Polym Sci Part C: Polym Symp 1960, 15, 263.
14. Yamaguchi, M.; Miyata, H.; Nitta, K.-H. J Appl Polym Sci 1996, 62, 87.
15. Muller, F. H.; Huff, K. Kolloid Z 1959, 166, 44.
16. Min, K.; White, J. L. Polym Eng Sci 1984, 24, 1327.
17. Ling, Z.; Rui, H.; Linagbin, L.; Gang, W. J Appl Polym Sci 2003, 83, 1870.
18. Kim, B. K.; Do, I. H. J Appl Polym Sci 1996, 60, 2207.
19. Zoller, P.; Walsh, P. J. Standard Pressure-Volume-Temperature Data for Polymers; Technomic Publishing Co: Lancaster PA; 1995.
20. Choy, C. L.; Chen, F. C.; Ong, E. L. Polymer 1979, 20, 191.
21. Choy, C. L.; Chen, F. C.; Young, K. J Polym Sci: Polym Phys Ed 1981, 19, 335.
22. Alexander, E. J. X-Ray Diffraction Methods in Polymer Science; Wiley-Science: New York; 1969.
23. Ran, S.; Hsiao, B. S.; Agarwal, P. K.; Varma-Nair, M. Polymer 2003, 44, 2385.